JIRSS (2024)
Vol. 23, No. 02, pp 179-197
DOI: 10.22034/jirss.2025.2028062.1060

Analytical Characterization of Dimple Effect for Spatio-temporal Beams

Ali M. Mosammam[1]

[1] Department of Statistics, University of Zanjan, Zanjan, Iran.

Received: 03/05/2024, Accepted: 06/06/2025, Published online: 24/06/2025

Abstract. In this paper, we first consider the propagation characteristics of a spatio-temporal Gaussian pulse using both simplified analytical and numerical approaches. Second, we focus on the counterintuitive presence of a possible dimple property associated with these spatio-temporal Gaussian pulses and the corresponding intensity functions. The analytical results are supported with numerical simulations of the exact pulsed-beam solution and various plots.

Keywords. Gaussian Beam, Dimple Effect, Parabolic Approximation, Wave Propagation.

MSC: 62M15, 62M30, 62H11.

1 Introduction

The characteristics of the spatio-temporal Gaussian beams are well known and can be found in a variety of literatures. In practice, controlling the beam shape is important not only in time but also in space. Campbell and DeShazer (1969) noticed that the shape of the output beam is affected by the finite size of the beam shaper apertures and by the beam's propagation. Ziolkowski and Judkins (1992) have studied the spatial and temporal behaviors of a femtosecond pulsed Gaussian beam and have found that the spread of the intensity and energy profiles differ.

In the context of this paper, the term distribution refers to the functional form describing the spatial and temporal intensity of the Gaussian beam, rather than a probability distribution for random variables. However, there is a strong analogy to

Corresponding Author: Ali M. Mosammam (a.m.mosammam@znu.ac.ir).

probability distributions, specifically the Gaussian distribution, which is foundational in statistics. In the physical sense the intensity distribution describes how energy is spread spatially and temporally across the beam. Mathematically, this intensity follows a Gaussian function, akin to a probability density function in statistics, where the spatial coordinates and time are treated as variables rather than random variables. If interpreted as a probability distribution, the moments (mean, variance, and higher moments) of the Gaussian function could correspond to physical properties. Mean represents the center or peak of the beam in space or time. Variance/Standard Deviation corresponds to the beam width (spatial spread) or pulse duration (temporal spread). This defines the region where the intensity is concentrated, analogous to how standard deviation measures dispersion in probability. For time-domain pulses, the duration of the Gaussian pulse is proportional to the standard deviation in time. This reflects how the pulse's energy spreads over time. As a Gaussian beam propagates, its spread increases, similar to how variance grows in statistical contexts involving convolution or integration over distributions.

An interesting feature in the beam is the appearance of a dimple on the axis in the corresponding intensity distribution. This effect is similar to the dip on the axis observed for truncated fundamental mode Gaussian beams (Campbell and DeShazer, 1969). The dimple has also been pointed out in studies by Degnan (1973); Stuut and Sargent (1984); Ohtsuka et al. (1985); Harris (1987); Matizen and Troitskiĭ (1987); Cazzoli et al. (1992); Aközbek et al. (2002); Hussain (2002); Gutiérrez-Vega and Bandres (2005); Chu et al. (2010); Zhou (2011); Tao et al. (2012); Yang et al. (2015); Franek et al. (2017) and DErrico et al. (2017). The dimple caused by the outcoupling mirror was pointed out by Hofstra et al. (1996), but they claim that this will not dramatically affect the focus profile. Lorenser et al. (2013) demonstrated use of the beam propagation method to analyze beam distortion in graded-index-lensed fibers resulting from index profiles that exhibit a deviation from the ideal parabolic shape or artifacts such as ripples or a dimple.

In this paper we discuss the basic properties of spatio-temporal Gaussian beams. The propagation characteristics of a spatio-temporal Gaussian pulse in a simple approach are considered both analytically and numerically. In particular, the spatial and temporal behaviors of a Gaussian beam are studied. We draw out attention on the counter-intuitive presence of possible dimple property associated with these spatio-temporal Gaussian pulses and the corresponding intensity functions. We identify the conditions under which the dimple effect appears, an effect that, to our knowledge, has not yet been studied analytically. This research may be useful for the practical applications of beams.

The Gaussian beam is the simplest case of laser beams in practical applications. For the sake of simplicity, we restrict our analysis to spatio-temporal Gaussian beams. As demonstrated in this paper, Gaussian beams behave in a very easy way. Its evolution are known and their characterization can be made with a few parameters. Some other types of beams include the Gaussian beam as the core of their amplitude profile. We

believe that similar effects typical to Gaussian beam can also be observed in other types of beams. For instance, the radial intensity profiles as a function of propagation distance of modes radiated at the waveguide termination are presented by Balkcum et al. (1992) to establish the antenna pattern of the waveguide. Zeng-Hui and Bai-Da (2008) have discussed the nonparaxial propagation of phase-flipped Gaussian beams. They noticed an on-axis dimple, in which width of the dimple increases with the increase of the propagation distance, and connected it to the behaviour of the error function at the origin. An extension of phase-flipped Gaussian beams to the multi-mode nonparaxial case is made by Gao and Lü (2007), where the intensity profile with or without dimple, interpreted straightforwardly. Propagation of ultrashort optical pulses in a linear optical medium has been studied extensively (Wang et al., 1997). The source field values are pre-calculated using an analytical description of a Gaussian beam modulated with a Gaussian pulse.

The general propagation equations of Hermite-cosh-Gaussian laser beams have been derived and illustrated with numerical examples by Belafhal and Ibnchaikh (2000). They noted that for small values of the decentered parameter or for large values of the mode index, a dimple appears and becomes important and with increasing the decentered parameter, the number of the lobes increases. The cosh-Gaussian beam diffracted by a circular aperture and passing through the turbulent atmosphere has been studied by (Chu et al., 2007).

Some extensions of the fundamental Bessel-Gauss beams, that may find practical applications, have been introduced and studied in free propagation by Bagini et al. (1996). They investigated, both analytically and numerically the behaviour of generalized Bessel-Gauss beams upon propagation. Walde et al. (2017) produced a Bessel beam illumination for multicolour and broad-spectrum imaging applications. The generated Bessel beam exhibits a pronounced central dip along the optical axis which is undesirable for practical purposes.

Convenient spatial-temporal Gaussian beam wave and its corresponding intensity and the dimple effect are developed in section 2. The corresponding spatio-temporal dimple are generalized in section 3. Finally, brief conclusions are given in section 4.

2 Spatio-temporal Monochromatic Beam Wave

Suppose that $f(x,z,t)$ is the function describing spatio-temporal distribution of the monochromatic wave amplitude in time and space defined as

$$f(x,z,t) = \Re\{\phi(x,z)\exp(i\tau_0 t)\}, \tag{2.1}$$

where the complex, in x direction spatially-bounded impulse-like, monochromatic amplitude distribution of the wave is given by $\phi(x,z)$ and τ_0 is the angular frequency of the harmonic oscillations. Here x represents the spatial coordinate perpendicular to the beam's propagation axis, z denotes the propagation distance along the beam's axis and t refers to time, which characterizes the temporal evolution of the beam pulse.

$\Re\{\cdot\}$ stands for the real part. We assume the z axis as the propagation direction of the laser beam. Next we introduce the "slowly varying envelope in propagation direction", $\bar{\phi}(x,z)$, by

$$\phi(x,z) = \bar{\phi}(x,z)\exp(-i\beta_0 z), \tag{2.2}$$

where the term $\exp(-i\beta_0 z)$ accounts for the wave oscillation along the propagation direction and strip-off the fast oscillations. Thus if the propagation direction is assumed to be along the z axis, this field has the form $f(x,z,t) = \Re\{\bar{\phi}(x,z)\exp(i\tau_0 t - i\beta_0 z)\}$. The phase of the wave takes the simple form $(\tau_0 t - \beta_0 z)$, where β_0 is the wave number and τ_0 is the angular frequency. It is known that for the wave amplitude distribution $f(x,z,t)$ in (2.1), the propagation of waves is given by the wave equation in form

$$\frac{\partial^2 f(x,z,t)}{\partial x^2} + \frac{\partial^2 f(x,z,t)}{\partial z^2} - \frac{1}{c^2}\frac{\partial^2 f(x,z,t)}{\partial t^2} = 0,$$

where $c = 1/\sqrt{\mu\varepsilon}$ is the phase velocity of wave propagation with permeability μ and permittivity ε. The amplitude $\phi(x,z)$ of a monochromatic wave in (2.2) takes the Helmholtz equation in form

$$\frac{\partial^2 \phi(x,z)}{\partial x^2} + \frac{\partial^2 \phi(x,z)}{\partial z^2} + \beta_0^2 \phi(x,z) = 0, \tag{2.3}$$

where $\beta_0 = \tau_0/c$ is the phase constant. By substituting (2.2) in (2.3) and simplifying we arrive instead of (2.3) to the wave equation for $\bar{\phi}(x,z)$ in the form

$$\frac{\partial^2 \bar{\phi}(x,z)}{\partial x^2} - 2i\beta_0 \frac{\partial \bar{\phi}(x,z)}{\partial z} + \frac{\partial^2 \bar{\phi}(x,z)}{\partial z^2} = 0.$$

Let $\Phi(\omega,z)$ be the inverse spatial Fourier transform pair of $\phi(x,z)$:

$$\phi(x,z) = \int_{-\infty}^{\infty} \Phi(\omega,z)\exp(-i\omega x)d\omega.$$

It then follows that the Helmholtz equation (2.3) in spectral domain may be written as

$$\frac{\partial^2 \Phi(\omega,z)}{\partial z^2} + (\beta_0^2 - \omega^2)\Phi(\omega,z) = 0.$$

The solution for the above wave propagating in the positive direction of the z-axis takes the form(Franek et al., 2017) $\Phi(\omega,z) = \Phi_0(\omega)\exp\left(-iz\sqrt{\beta_0^2 - \omega^2}\right)$, where $\Phi_0(\omega)$ is the Fourier transform of the initial value $\phi_0(x) = \phi(x,z)|_{z=0}$, thus

$$\phi(x,z) = \int_{-\infty}^{\infty} \Phi_0(\omega)\exp\left(-iz\sqrt{\beta_0^2 - \omega^2}\right)\exp(-i\omega x)d\omega. \tag{2.4}$$

Although an analytical expression for (2.4) is not directly available, it can be reasonably approximated by applying $\sqrt{\beta_0^2 - \omega^2} \approx \beta_0 - \omega^2/2\beta_0$, so instead of (2.4) one arrives at the inverse Fourier transform formula in the form

$$\phi(x,z) = \exp(-i\beta_0 z) \int_{-\infty}^{\infty} \Phi_0(\omega) \exp\left(-i\omega^2 z/2\beta_0\right) \exp(-i\omega x) d\omega. \tag{2.5}$$

This approximation considerably simplifies the analytical integration of the Fourier integrals. The integral in (2.5) is in fact the solution of the following equation in the spatial-frequency domain

$$\frac{\partial \bar{\Phi}(\omega,z)}{\partial z} - \frac{i\omega^2}{2\beta_0} \bar{\Phi}(\omega,z) = 0, \tag{2.6}$$

where $\bar{\Phi}(\omega,z)$ is the Fourier transform of $\bar{\phi}(x,z)$ with the initial condition $\bar{\phi}(\omega,z)|_{z=0} = \phi_0(\omega)$. The transformation of (2.6) into the spatial domain yields the parabolic partial differential equation

$$\frac{\partial^2 \bar{\phi}(x,z)}{\partial x^2} - 2i\beta_0 \frac{\partial \bar{\phi}(x,z)}{\partial z} = 0.$$

For the initial Gaussian wave-amplitude profile $\phi_0(x)$ with the spatial spectrum

$$\Phi_0(\omega) = \frac{W_{x_0}}{\sqrt{2\pi}} \exp(-\omega^2 W_{x_0}^2/2),$$

where W_{x_0} denotes the effective width, and performing the inverse transforms analytically, the propagating monochromatic Gaussian beam wave from (2.5) takes the form

$$\begin{aligned}
\bar{\phi}(x,z) &= \int_{-\infty}^{\infty} \frac{W_{x_0}}{\sqrt{2\pi}} \exp(-\omega^2 W_{x_0}^2/2) \exp\left(-i\omega^2 z/2\beta_0\right) \exp(-i\omega x) d\omega \\
&= \frac{W_{x_0}}{\sqrt{W_{x_0}^2 - iz/\beta_0}} \exp\left(-\frac{x^2}{2(W_{x_0}^2 + iz/\beta_0)}\right) \\
&= \frac{1}{\sqrt{1 - iz\alpha_0}} \exp\left(-\frac{\beta_0}{2} \frac{\alpha_0 x^2}{1 - iz\alpha_0}\right) \\
&= \frac{1}{\sqrt{1 - iz\alpha_0}} \exp\left(-\frac{x^2}{2W_x^2}\right) \exp\left(i\beta_0 \frac{x^2}{2R_x}\right),
\end{aligned} \tag{2.7}$$

where $\alpha_0 = 1/\beta_0 W_{x_0}^2$, $W_x = W_x(z) = W_{x_0}\sqrt{1 + z^2\alpha_0^2}$ is the effective width (waist) of the beam wave and $R_x = R_x(z) = -z(1 + 1/(\alpha_0 z)^2)$ is the radius of the wavefront curvature after propagating a distance on the z-axis, both in the plane z =const. Both are functions of the propagation path z. $R_x(z)$ tends to ∞ as z approaches zero, passes through a minimum at some finite z, and rises again toward infinity as z is further increased, asymptotically approaching the value of z itself.

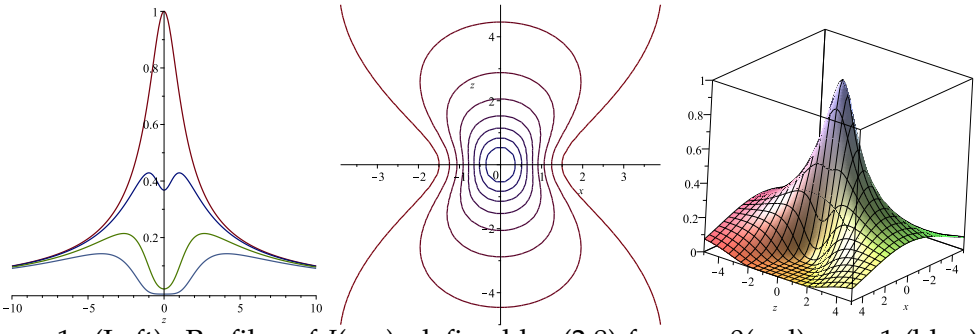

Figure 1: (Left): Profiles of $I(x,z)$, defined by (2.8) for $x = 0$(red), $x = 1$ (blue), $x = 2$ (green), $x = 3$ (light blue). (Middle): Contour map of the intensity profiles, $I(x,z)$, defined by (2.8). (Right): perspective plot of the intensity profiles, $I(x,z)$, defined by (2.8). x is the distance from the optical axis, and z is the propagation distance. In this case, $\alpha_0 = 1, \beta_0 = 1$. A dimple is seen for $|x| > \sqrt{2}/2$.

2.1 Dimple Effect of Monochromatic Beam Wave

The intensity of the monochromatic beam field, using the properties of complex conjugates, is readily obtained as the absolute square of (2.7)

$$\begin{aligned} I(x,z) = |\bar{\phi}(x,z)|^2 &= \frac{1}{\sqrt{\alpha_0\beta_0}W_x(z)} \exp\left(-\frac{x^2}{W_x^2(z)}\right) \\ &= \frac{1}{\sqrt{1+z^2\alpha_0^2}} \exp\left(-\frac{x^2}{W_{x_0}^2(1+z^2\alpha_0^2)}\right) \\ &= \frac{1}{\sqrt{1+z^2\alpha_0^2}} \exp\left(-\frac{\beta_0\alpha_0 x^2}{1+z^2\alpha_0^2}\right). \end{aligned} \tag{2.8}$$

If one considers (2.8) it is easily seen, that the profile of the wave intensity is a symmetrical Gaussian function for the transversal variable x and also for the propagation variable z (see Fig. 1(Right)). In other worlds, the spatio-temporal wave $f(x,z,t)$, (2.1), has a "fully symmetric" intensity structure, (2.8), that is the following condition holds,

$$I(x,z) = I(-x,z) = I(x,-z) = I(-x,-z) \quad \text{for all} \quad (x,z).$$

As the transversal variable x or the propagation variable z increases, we typically expect the intensity to decrease and approach zero for large distances. But in this paper we draw out attention on the counter-intuitive presence of possible dimple property associated with the intensity surface (2.8) which contradicts the natural monotonicity structure of intensity. An interesting feature in the intensity is the appearance of a dimple on z-axis in the intensity distribution: the intensity function $I(x,z)$, defined by (2.8), has a dimple in the z-axis if there exists a real value $x^* > 0$ such that the following properties hold.

- (a) For fixed $|x| \leq x^*$, $I(x,z)$ is increasing in $z \leq 0$ and decreasing in $z \geq 0$.
- (b) For fixed $|x| > x^*$, $I(x,z)$ is increasing for $z \in (-\infty, -z^*)$, decreasing for $z \in (-z^*, 0)$, increasing for $z \in (0, z^*)$, and decreasing for $z \in (z^*, \infty)$ for some $z^* = z^*(x) > 0$, depending on x.

We now investigates the circumstances under which (2.8) will possess a dimple. Taking partial derivative of (2.8) with respect to z, and indicating the derivation with a prime, we obtain

$$\frac{\partial}{\partial z} I(x,z) = \frac{W_x'(z) \exp\left(-\frac{x^2}{W_x^2(z)}\right)}{\sqrt{\alpha_0 \beta_0} W_x^2(z)} \left(\frac{2x^2}{W_x^2(z)} - 1\right). \tag{2.9}$$

Since $W_x(\infty) = \infty$ and $W_x'(\infty) = 1$, $\frac{\partial}{\partial z} I(x,z)$ tends to zero in the far zone and since $W_x'(0) = 0$, it vanishes for $z = 0$. It can also vanish when $\left(\frac{2x^2}{W_x^2(z)} - 1\right) = 0$. For $\frac{2x^2}{W_x^2(z)} < 1$, $\frac{\partial}{\partial z} I(x,z)$ is negative for all $z > 0$. If $|x| > \sqrt{2}/2 W_x(z)$, then $\frac{\partial}{\partial z} I(x,z)$ is positive for $z \in (0, z^*)$ and negative for $z \in (z^*, \infty)$, where $z^* = W_x^{-1}(\sqrt{2}x)$. Since $I(x,z)$ is fully symmetric, these are precisely the conditions (a) and (b) given above for a dimple to exist. Hence, given $W_x(z) = W_{x_0}\sqrt{1 + z^2 \alpha_0^2}$ the longitudinal intensity profile as a function of the variable z reveals dimple for $|x| > 1/\sqrt{2\alpha_0 \beta_0}$. The height of a dimple takes the value $I(x^*, 0)/I(0,0) = \exp(-\alpha_0 \beta_0 x^{*2}) = \exp(-1/2)$. For more details of the dimple property in the spatio-temporal covariance function see Kent et al. (2011). See also Mohammadzadeh et al. (2015) to information of how to avoid the dimple in spatio-temporal covariance functions.

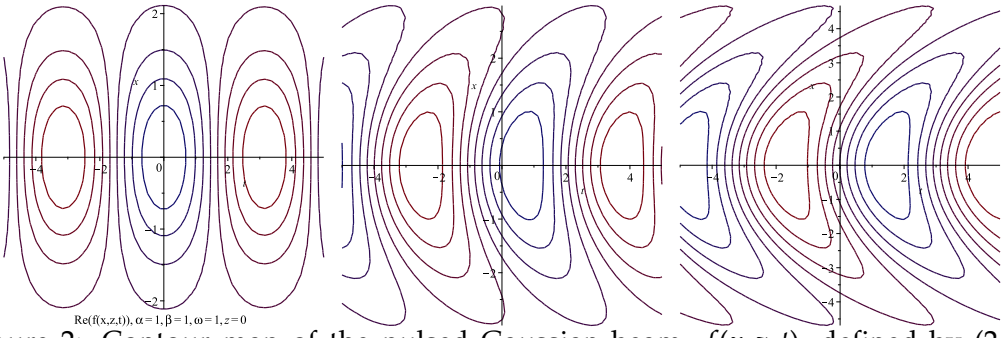

Figure 2: Contour map of the pulsed Gaussian beam, $f(x,z,t)$, defined by (2.1) as observed on the planes: (Left) $z = 0$, (Middle) $z = 1$, (Right) $z = 2$. x is the distance from the optical axis, and t is the relative time. In this case, $\alpha_0 = 1$, $\beta_0 = 1$, $\tau_0 = 1$.

For (2.8) the dimple effects are illustrated in Figure 1. Here and in the following, the intensity is measured in arbitrary units. From Figure 1(Left), we can see that for a

small value $|x| < \sqrt{2}/2$, the one-dimensional intensity profile of the beam is similar to a Gaussian distribution (without a dimple) and, with x increasing, the profile becomes flat-topped ($|x| = \sqrt{2}/2$). Moreover, with x further increasing ($|x| > \sqrt{2}/2$), the dimple appears, and becomes larger and deeper. Meanwhile, the peak values of the one-dimensional intensity at the z-plane all decrease and the width of the dimple increases with the increase of the distance x.

It is interesting to note that the intensity function inherited the dimple effect from the corresponding wave. The spatio-temporal contour map of the pulse of propagation in free space are demonstrated in Figure 2 and it is shown in Figure 3 that as the pulse propagates from near to far field, the transverse spatial shape reveals negative value, dimple and reverse dimple effect with the wave front. A wave can be negative in x axis for some z and t exhibiting one or more oscillations before approaching zero. We refer to Mosammam (2015) for accurate definition of negative value and reverse dimple effect.

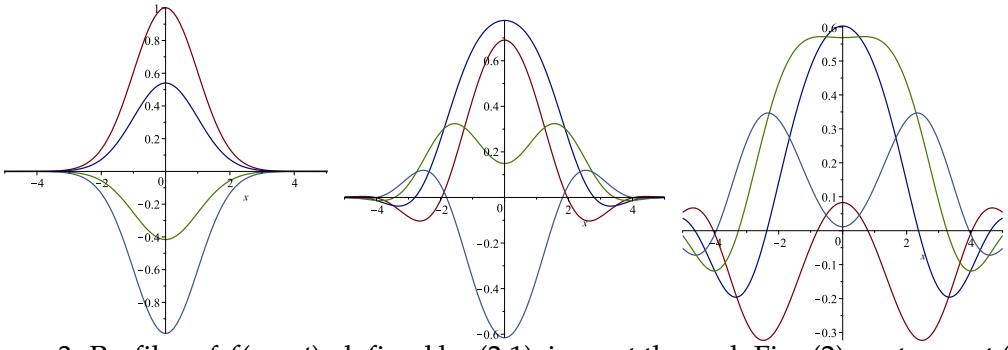

Figure 3: Profiles of $f(x, z, t)$, defined by (2.1), ie a cut through Fig. (2) contours at (Left) $z = 0$, (Middle) $z = 1$, (Right) $z = 2$, for $t = 0$(red), $t = 1$(blue), $t = 2$(green), $t = 3$(light blue). x is the distance from the optical axis. In this case, $\alpha_0 = 1$, $\beta_0 = 1$, $\tau_0 = 1$.

3 Spatio-temporal Electromagnetic Beam Wave

We adopt one-dimensional intensity functions in the numerical calculation and analysis for simplicity. The properties of one-dimensional intensity functions can reflect the properties of a two-dimensional intensity function as well. Next consider the spatial-temporal electromagnetic beam wave

$$f(x, z, t) = \Re\{\bar{\psi}(x, z, t) \exp(i\tau_0 t - i\beta_0 z)\}, \tag{3.1}$$

where $\psi(x, z, t) = \bar{\psi}(x, z, t) \exp(-i\beta_0 z)$ is the spatial and temporal impulse complex "slowly varying amplitude-envelope in time" of the wave. Then the spatial-temporal Helmholtz equation takes the form

$$\frac{\partial^2 \psi(x, z, t)}{\partial x^2} + \frac{\partial^2 \psi(x, z, t)}{\partial z^2} - \frac{1}{c^2} \frac{\partial^2 \psi(x, z, t)}{\partial t^2} - \frac{2i\beta_0}{c} \frac{\partial \psi(x, z, t)}{\partial t} + \beta_0^2 \psi(x, z, t) = 0,$$

or equivalently in the form

$$\frac{\partial^2\bar{\psi}(x,z,t)}{\partial x^2}+\frac{\partial^2\bar{\psi}(x,z,t)}{\partial z^2}-\frac{1}{c^2}\frac{\partial^2\bar{\psi}(x,z,t)}{\partial t^2}-2i\beta_0\left(\frac{\partial\bar{\psi}(x,z,t)}{\partial z}+\frac{1}{c}\frac{\partial\bar{\psi}(x,z,t)}{\partial t}\right)=0.$$

The Helmholtz equation in the spatial-temporal spectral domain takes the form

$$\frac{\partial^2\Psi(\omega,z,\tau)}{\partial z^2}+\{(\beta_0+\tau/c)^2-\omega^2\}\Psi(\omega,z,\tau)=0.$$

The solution for the wave propagating in the positive direction of the z-axis takes the form (Franek et al., 2017) $\Psi(\omega,z,\tau)=\Psi_0(\omega,\tau)\exp\left(-iz\sqrt{(\beta_0+\tau/c)^2-\omega^2}\right)$, where $\Psi(\omega,z,\tau)$ is the two-dimensional spatial-temporal Fourier transform of $\psi(x,z,t)$ with initial value $\Psi_0(\omega,\tau)$, thus leading to the formula

$$\psi(x,z,t)=\int\int\Psi_0(\omega,\tau)\exp\left(-iz\sqrt{(\beta_0+\tau/c)^2-\omega^2}\right)\exp\left(i\tau t-i\omega x\right)d\omega d\tau. \tag{3.2}$$

Parabolic approximation can be used also for spatial-temporal wave by applying $\sqrt{(\beta_0+\tau/c)^2-\omega^2}\approx\beta_0+\tau/c+\tau^2/2c^2\beta_0-\omega^2/2\beta_0$ (this approximation considerably simplifies the analytical integration of the Fourier integrals), resulting in the form

$$\psi(x,z,\tau)=\exp(-i\beta_0 z)\int\int\Psi_0(\omega,\tau)\exp\left(iz[\omega^2-(\tau/c)^2]/2\beta_0\right)\exp\left(i[\tau t-\omega x]\right)d\omega d\tau, \tag{3.3}$$

where $\tau=t-z/c$ is the retarded time. This result is also the solution of

$$\frac{\partial\bar{\Psi}(\omega,z,\tau)}{\partial z}+i\{\omega^2/2\beta_0-\tau^2/2\beta_0c^2-\tau/c\}\bar{\Psi}(\omega,z,\tau)=0,$$

in the frequency domain, where $\bar{\Psi}(\omega,z,\tau)$ is the two-dimensional spatial-temporal Fourier transform of $\bar{\psi}(x,z,t)$ with initial value $\bar{\Psi}_0(\omega,\tau)$. This corresponds to the parabolic equation

$$\frac{\partial^2\bar{\psi}(x,z,t)}{\partial x^2}-2i\beta_0\frac{\partial\bar{\psi}(x,z,t)}{\partial z}-\frac{1}{c^2}\frac{\partial^2\bar{\psi}(x,z,t)}{\partial t^2}-\frac{2i\beta_0}{c}\frac{\partial\bar{\psi}(x,z,t)}{\partial t}=0. \tag{3.4}$$

For the retarded time $\tau=t-z/c$ and $\bar{\psi}(x,z,\tau)=\bar{\psi}(x,z,t-z/c)$ the resulting parabolic equation instead of (3.4) may be written as

$$\frac{\partial^2\bar{\psi}(x,z,\tau)}{\partial x^2}-2i\beta_0\frac{\partial\bar{\psi}(x,z,\tau)}{\partial z}-\frac{1}{c^2}\frac{\partial^2\bar{\psi}(x,z,\tau)}{\partial\tau^2}=0.$$

Using (3.3) let us consider the propagation of an electromagnetic wave with gaussian spatial and temporal modulation at $z=0$. In a special case of a spatial-temporal wave-packet, i.e of a Gaussian distribution of the amplitude-envelope in time and space with the spatial-temporal spectrum

$$\Psi_0(\omega,\tau)=\frac{W_{x_0}W_{t_0}}{2\pi}\exp(-\omega^2W_{x_0}^2/2)\exp(-\tau^2W_{t_0}^2/2), \tag{3.5}$$

formula (3.3) yields separable spatial-temporal inverse Fourier integrals

$$\begin{aligned}\bar{\psi}(x,z,t-z/c) &= \frac{W_{x_0}W_{t_0}}{2\pi}\int_{-\infty}^{\infty}\exp(-\omega^2W_{x_0}^2/2)\exp\left(-i\omega^2 z/2\beta_0\right)\exp(-i\omega x)d\omega\\ &\times\int_{-\infty}^{\infty}\exp(-\tau^2W_{t_0}^2/2)\exp\left(-i\tau^2 z/2\beta_0c^2\right)\exp(-i\tau(t-z/c))d\tau\\ &= \frac{1}{\sqrt{1-iz\alpha_0}}\exp\left(-\frac{\beta_0}{2}\frac{\alpha_0x^2}{1-iz\alpha_0}\right)\frac{1}{\sqrt{1+iz\chi_0}}\exp\left(-\frac{c^2\beta_0}{2}\frac{\chi_0(t-z/c)^2}{1+iz\chi_0}\right)\\ &= \frac{1}{\sqrt{1-iz\alpha_0}}\exp\left(-\frac{x^2}{2W_x^2}\right)\exp\left(i\beta_0\frac{x^2}{2R_x}\right)\\ &\times\frac{1}{\sqrt{1+iz\chi_0}}\exp\left(-\frac{(t-z/c)^2}{2W_t^2}\right)\exp\left(ic^2\beta_0\frac{(t-z/c)^2}{2R_t}\right),\end{aligned}\tag{3.6}$$

where $\chi_0 = 1/c\tau_0W_{t_0}^2$, the effective width of the beam wave in time domain is $W_t = W_{t_0}\sqrt{1+z^2\chi_0^2}$, and $R_t = -z(1+1/(\chi_0 z)^2)$ characterises the non-linear phase modulation of the pulse. Both are functions of the propagation path z.

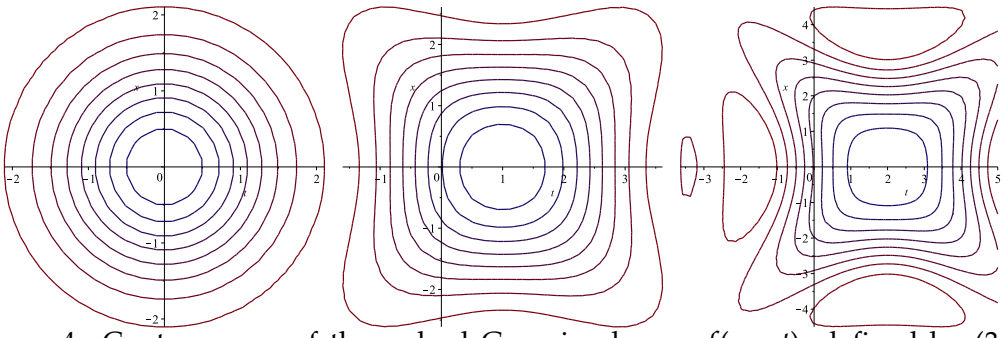

Figure 4: Contour map of the pulsed Gaussian beam, $f(x,z,t)$, defined by (3.1) as observed on the planes: (Left) $z = 0$, (Middle) $z = 1$, (Right) $z = 2$. x is the distance from the optical axis, and t is the relative time. In this case, $\chi_0 = 1$, $\alpha_0 = 1$, $\beta_0 = 1$, $c = 1$.

3.1 Dimple Effect of Electromagnetic Beam Wave

Next the spatio-temporal profiles of a spatio-temporal electromagnetic Gaussian pulse are studied. In practice, controlling the pulse shape is important not only in time but also in space. It is found from (3.6) that the temporal time shape of the pulse on propagation is also in Gaussian form and the pulsewidth is unchanged on propagation, but in comparison with that of the waist, the field contains a retarded time given by $t = z/c$ which is related with the wavefront, i.e., the peak of the pulse propagates with the wavefront. Hence, the peaks of the paraxial pulses have a delay in comparison with that of the on-axis pulses. Besides the temporal analyses, the space behavior of

the field is interesting too. In addition there are negative value, dimple and reverse dimple effects in the pulse. We see that, increasing the propagation of the pulse, an oscillating behaviour appears and becomes more and more evident. For clearer illustration of these behaviors, the on-axis wave $f(x,z,t)$ is graphed versus x and time in Figures (5) and (6), respectively and for the z locations $z = 0, 1$, and 2. This sequence clearly demonstrates the evolution of the initial Gaussian pulse as the beam propagates farther from the origin. Similar behaviour is seen in the phase part of the pulse.

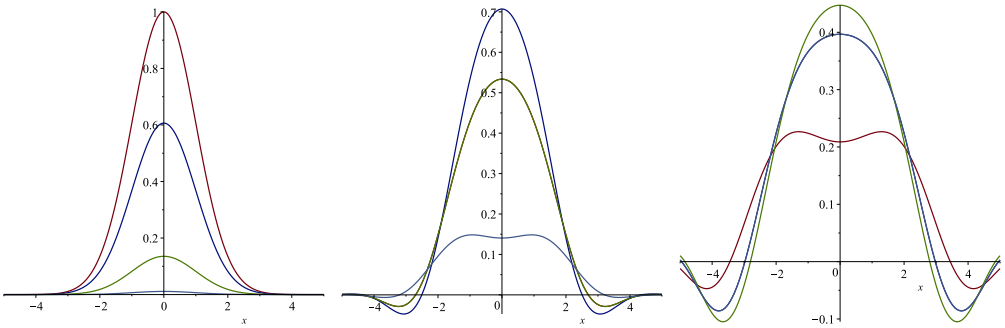

Figure 5: Profiles of $f(x,z,t)$, defined by (3.1), ie a cut through Fig. (4) contours at (Left) $z = 0$, (Middle) $z = 1$, (Right) $z = 2$, for $t = 0$ (red), $t = 1$ (blue), $t = 2$ (green), $t = 3$ (light blue). x is the distance from the optical axis. In this case, $\chi_0 = 1$, $\alpha_0 = 1$, $\beta_0 = 1$, $c = 1$.

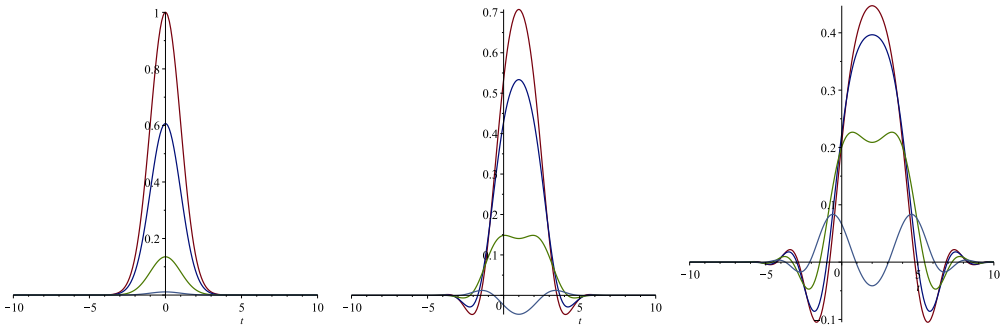

Figure 6: Profiles of $f(x,z,t)$, defined by (3.1), ie a cut through Fig. (4) contours at (Left) $z = 0$, (Middle) $z = 1$, (Right) $z = 2$, for $x = 0$ (red), $x = 1$ (blue), $x = 2$ (green), $x = 3$ (light blue). t is the relative time. In this case, $\chi_0 = 1$, $\alpha_0 = 1$, $\beta_0 = 1$, $c = 1$.

If we set $z = 0$, the pulsed wave field at the waist turns out to be

$$\bar{\psi}(x,t) = \exp\left(-\frac{\beta_0}{2}\alpha_0 x^2\right)\exp\left(-\frac{c^2\beta_0}{2}\chi_0 t^2\right),$$

which is the inverse Fourier transform of (3.5). In this paper, for simplicity, the initial input pulses, it is assumed that the space and time field components of the pulse can

be separated. The intensity of the beam determined by squaring (3.6):

$$\begin{aligned} I(x,z,t-z/c) &= |\bar{\psi}(x,z,t-z/c)|^2 \\ &= \frac{1}{\sqrt{(1+z^2\alpha_0^2)(1+z^2\chi_0^2)}} \exp\left(-\frac{\beta_0\alpha_0 x^2}{1+z^2\alpha_0^2} - \frac{\beta_0 c^2(t-z/c)^2}{1+z^2\chi_0^2}\right) \\ &= \frac{1}{c\beta_0\sqrt{\alpha_0\chi_0}W_t(z)W_x(z)} \exp\left(-\frac{x^2}{W_x^2(z)} - \frac{(t-z/c)^2}{W_t^2(z)}\right). \end{aligned} \tag{3.7}$$

The intensity function $I(x,z,t-z/c)$, defined by (3.7), has a dimple in the z axis if there exist two real value $x^*, t^* > 0$ such that the following properties hold.

- (a) For fixed $|t| \le t^*$ and $|x| \le x^*$, $I(x,z,t-z/c)$ is increasing in $z \in (-\infty, z_2^*)$ and decreasing in $z \in (z_2^*, \infty)$. (If $t=0$, then $I(x,z,t-z/c)$ is fully symmetric and $z_2^* = 0$)

- (b) For fixed $|t| \le t^*$ and $|x| > x^*$, $I(x,z,t-z/c)$ is increasing for $z \in (-\infty, z_1^*)$, decreasing for $z \in (z_1^*, z_2^*)$, increasing for $z \in (z_2^*, z_3^*)$ and decreasing for $z \in (z_3^*, \infty)$ for some $z_1^* < z_2^* < z_3^*$, depending on x and t. (If $t=0$, then $I(x,z,t-z/c)$ is fully symmetric, $z_1^* = -z_3^*$ and $z_2^* = 0$)

- (c) For fixed $|t| > t^*$ and $|x| \ge 0$, $I(x,z,t-z/c)$ is increasing for $z \in (-\infty, z_1^*)$, decreasing for $z \in (z_1^*, z_2^*)$, increasing for $z \in (z_2^*, z_3^*)$ and decreasing for $z \in (z_3^*, \infty)$ for some $z_1^* < z_2^* < z_3^*$, depending on x and t.

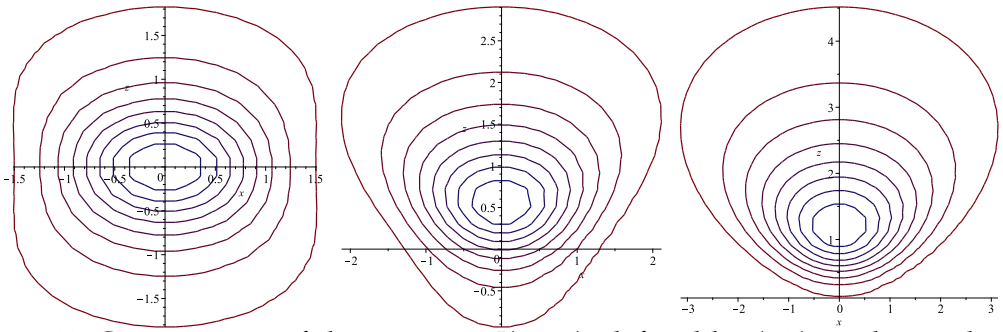

Figure 7: Contour map of the intensity, $I(x,z,t)$, defined by (3.7) as observed on the planes: (Left) $t=0$, (Middle) $t=1$, (Right) $t=2$. x is the distance from the optical axis, z is the propagation distance. In this case, $\chi_0 = 1$, $\alpha_0 = 1$, $\beta_0 = 1$, $c = 1$.

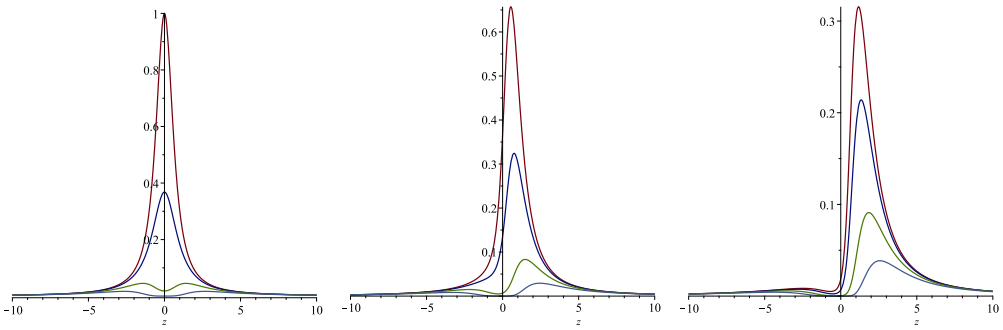

Figure 8: Profiles of the intensity, $I(x,z,t)$, defined by (3.7), ie a cut through Fig. (7) contours at (Left) $t = 0$, A dimple is seen for $|x| > \sqrt{2}$ (Middle) $t = 1$, A dimple is seen for $|x| > \sqrt{2}$ (Right) $t = 2$, A dimple is seen for $|x| \geq 0$, for $x = 0$(red), $x = 1$(blue), $x = 2$(green), $x = 3$(light blue). For $|t| \geq 1.673648$ for each $|x| \geq 0$ a dimple is seen. z is the distance propagation. In this case, $\chi_0 = 1$, $\alpha_0 = 1$, $\beta_0 = 1$, $c = 1$.

An intensity function is called axially symmetric in the transversal variable x if $I(x,z,t) = I(-x,z,t)$. Finally, an intensity function is called diagonally symmetric if $I(x,z,t) = I(x,-z,-t)$. If $t = 0$, then $I(x,z,t)$ is fully symmetric.

It is found from (3.7) that the wavefront also enters the expression of the intensity distribution of the pulse. In the following, we will apply these expressions to analyze the spatio-temporal profiles of the pulse propagating in free space. A more quantitative intensity profile can be examined by plotting a longitudinal cross section of the intensity profile. This distribution is displayed in Figure 8 for three different pulse durations, corresponding to three different values of the parameter t: from the shortest duration to the longest. From Figure 8 we can see that for a small values of t and x, the profile becomes a profile that bears some resemblance to the intensity profile of a Gaussian beam. For $t = 0$ and $|x| > \sqrt{2}$, the dimple of the intensity profile at the z-plane appears (see Figure 8(Left)). For $t = 1$ and $|x| > \sqrt{2}$, the dimple begins to appear (see Figure 8(Middle)). For $|t| \geq 1.673648$ and for each $|x| \geq 0$, the dimple appears (see Figures 8(Right). Meanwhile, the peak values of the one-dimensional intensity at the z-plane all move toward the right-hand (or left-hand depending on the sign of t) and decrease.

Let us now consider the intensity at $x = 0$ as a function of the longitudinal coordinate z. If one considers (3.7), it is easily seen that the profile of the wave intensity is a symmetrical Gaussian function for the transversal variable x. However, the longitudinal intensity profile as a function of the variable z or t is not symmetrical, ie is given as

$$I(x,z,t-z/c)_{x=0} = \frac{1}{\sqrt{(1+z^2\alpha_0^2)(1+z^2\chi_0^2)}} \exp\left(-\frac{\beta_0 c^2 (t-z/c)^2}{1+z^2\chi_0^2}\right), \tag{3.8}$$

and shown in Figure 10 (Left). In fact the intensity function (3.7) is axially symmetric in the transversal variable x and diagonally symmetric in z and t. If $t = 0$, then it is fully symmetric.

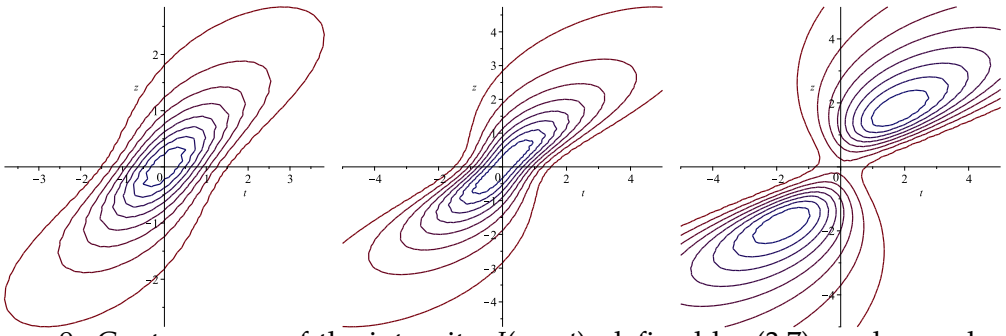

Figure 9: Contour map of the intensity, $I(x, z, t)$, defined by (3.7) as observed on the planes: (Left) $x = 0$, (Middle) $x = 1$, (Right) $x = 2$. t is the time, z is the propagation distance. In this case, $\chi_0 = 1$, $\alpha_0 = 1$, $\beta_0 = 1$, $c = 1$.

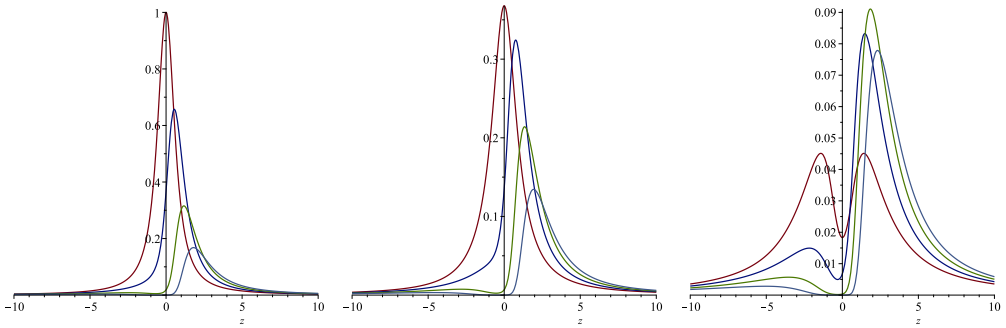

Figure 10: Profiles of the intensity, $I(x, z, t)$, defined by (3.7), ie a cut through Fig. (7) contours at (Left) $x = 0$, A dimple is seen for $|t| > 1.673647304$ (Middle) $x = 1$, A dimple is seen for $|t| > 1.38934636$ (Right) $x = 2$, A dimple is seen for $|t| \geq 0$, for $t = 0$ (red), $t = 1$ (blue), $t = 2$ (green), $3 = 3$ (light blue). For $|x| > \sqrt{2}$ for each $|t| \geq 0$ a dimple is seen. z is the distance propagation. In this case, $\chi_0 = 1$, $\alpha_0 = 1$, $\beta_0 = 1$, $c = 1$.

3.2 Dimple Effect in Peak Intensity and Energy Function

Because the transverse spatial shape of the pulse on propagation has dimple and negative value effects in the wavefront, the intensity distribution is very complicated. Because the intensity depends on time, it has limited usefulness. A more descriptive quantity is the maximum of the intensity in time. We first consider the peak intensity distribution defined on the plane where the intensity of the pulse on axis reached

maximum. Setting the partial derivative with respect to time of the electric fields given by relation (3.6) to zero, one finds that the maxima of the electric field are located at the time $t_{\max} = z/c$. The peak of the pulse on axis propagates from the waist to the certain plane the retarded time changes from zero to $t_{\max} = z/c$, so that the maximum intensity received at an observation point is

$$\Lambda_{\max}(x,z) = \max_{t} I(x,z,t-z/c) \quad = \quad \frac{1}{\sqrt{(1+z^2\alpha_0^2)(1+z^2\chi_0^2)}} \exp\left(-\frac{\beta_0\alpha_0 x^2}{1+z^2\alpha_0^2}\right). \quad (3.9)$$

Consequently, the ratio of the maximum intensity along the axis of propagation to the maximum intensity on axis at the aperture $z = 0$ is

$$\frac{\Lambda_{\max}(x=0,z)}{\Lambda_{\max}(x=0,z=0)} = \frac{1}{\sqrt{(1+z^2\alpha_0^2)(1+z^2\chi_0^2)}}. \quad (3.10)$$

Similarly, the ratio of the maximum intensity at a point in a plane orthogonal to the axis of propagation to its value on that axis will be

$$\frac{\Lambda_{\max}(x,z)}{\Lambda_{\max}(x=0,z)} = \exp\left(-\frac{\beta_0\alpha_0 x^2}{1+z^2\alpha_0^2}\right). \quad (3.11)$$

It is more useful to integrate the intensity over time and consider the spatial distribution of the pulse energy. The energy is obtained by integrating the intensity over all time:

$$\Xi(x,z) = \int_{-\infty}^{\infty} |\psi(x,z,t-z/c)|^2 dt = \frac{\sqrt{\pi}}{c\sqrt{\beta_0\chi_0}} \frac{1}{\sqrt{1+z^2\alpha_0^2}} \exp\left(-\frac{\beta_0\alpha_0 x^2}{1+z^2\alpha_0^2}\right). \quad (3.12)$$

Consequently, the ratio of the energy along the axis of propagation to the energy on axis at the aperture $z = 0$ is

$$\frac{\Xi(x=0,z)}{\Xi(x=0,z=0)} = \frac{1}{\sqrt{1+z^2\alpha_0^2}}.$$

Similarly, the ratio of the energy at a point in a plane orthogonal to the axis of propagation to its value on that axis is

$$\frac{\Xi(x,z)}{\Xi(x=0,z)} = \exp\left(-\frac{\beta_0\alpha_0 x^2}{1+z^2\alpha_0^2}\right).$$

Now we would like to characterize the maximum intensity and energy in term of the dimple effect. Figure 11 shows the values of the pulsed beam's maximum intensity and energy in the plane $z = 0, 1, 2$. As indicated by a comparison of Equations (3.9) and (3.12), the profile of the maximum intensity of the pulsed beam is narrower than the

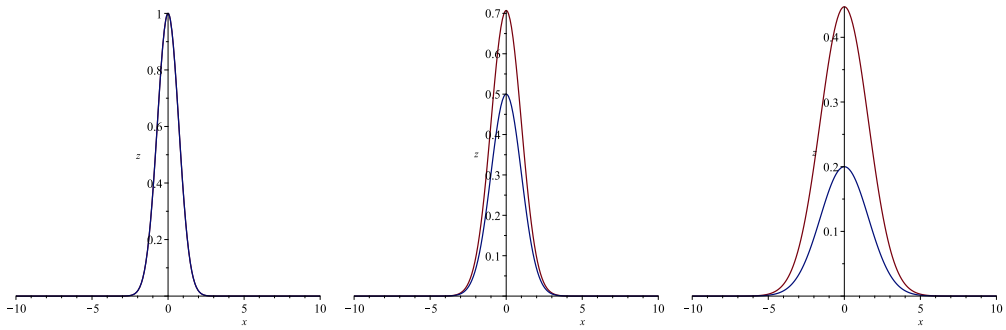

Figure 11: Profiles of the peak intensity (blue), $\Lambda_{\max}(x,z)$, defined by (3.9) and the energy (red) defined by (3.12) (Left) $z = 0$, (Middle) $z = 1$, (Right) $z = 2$. In this case, $\chi_0 = 1$, $\alpha_0 = 1$, $\beta_0 = 1$, $c = 1$.

corresponding beam-energy profile. Similar to (2.8), it is easily seen, that the profile of the wave energy (3.12) is a symmetrical Gaussian function for the transversal variable x and also for the propagation variable z. However, the longitudinal energy profile as a function of the variable z reveals dimple for $|x| > 1/\sqrt{2\alpha_0\beta_0}$. It is found from (3.9) and (3.12) that the dimple effect of intensity is different from the energy dimple effect, and that has been also mentioned in Figure 12. Finally, in Figure 12 we show the profiles of the peak intensity(blue), $\Lambda_{\max}(x,z)$, defined by (3.9) and the energy(red) defined by (3.12) of a beam as a function of z, at various planes. We see that, for the given choice of the parameters $\chi_0 = \alpha_0 = \beta_0 = c = 1$, the peak intensity and the energy distribution resembles that of the Gaussian beam at $|x| \leq \sqrt{2}/2$. As the distance increases, the energy and the peak intensity distributions assume a dimple for $|x| > \sqrt{2}/2$ and $|x| > 1$, respectively. It is found that at $|x| \leq \sqrt{2}/2$ the peak intensity profile is identical with the energy profile but when $|x| > \sqrt{2}/2$ because of the dimple effect, the peak intensity profile is smaller than the energy profile.

4 Conclusions

In conclusion, the most important properties of the spatio-temporal Gaussian pulse are summarized in this paper. Some aspects and critical features of the spatio-temporal wave propagation had been thoroughly discussed. In parabolic approximation the exact analytical results for a spatio-temporal Gaussian pulse can be obtained. The analytical results are supported with numerical simulations of the beam solution. A numerical investigation was undertaken to study the evolution of the Gaussian beam as it propagates away from the origin, i.e., as time or distance increases.

The evolution behaviors of intensity distributions of spatio-temporal Gaussian beams are considered. We show that in certain circumstances such spatio-temporal Gaussian pulses and corresponding intensity distributions possess a dimple. It is

shown analytically with an approximate form of the solution that the beam peak intensity and the beam energy have different dimple effect points. It is necessary to check for dimple effects in practice and include any necessary correction needed in spatio-temporal beams. The Gaussian beam case is treated in this paper because of its simplicity. We believe that similar effects typical to Gaussian beam can be observed in other types of beams.

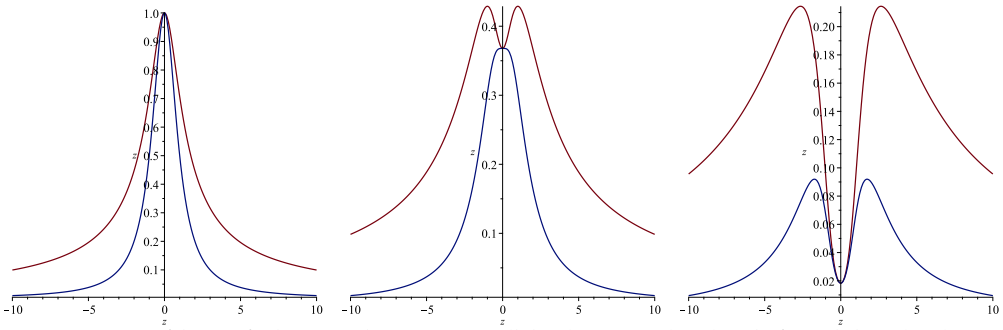

Figure 12: Profiles of the peak intensity(blue), $\Lambda_{\max}(x, z)$, defined by (3.9) and the energy(red) defined by (3.12) (Left) $x = 0$, (Middle) $x = 1$, (Right) $x = 2$. Dimple is seen in the energy for $x > \sqrt{2}/2$ and in the peak intensity for $x > 1$. In this case, $\chi_0 = 1$, $\alpha_0 = 1$, $\beta_0 = 1$, $c = 1$.

Acknowledgement

The author would like to thank the Editor-in-Chief, associate editor and referees, whose comments have been very helpful in improving the manuscript.

References

Aközbek, N., Bowden, C., and Chin, S. (2002). Propagation dynamics of ultra-short high-power laser pulses in air: supercontinuum generation and transverse ring formation. *journal of modern optics*, **49**(3-4), 475–486.

Bagini, V., Frezza, F., Santarsiero, M., Schettini, G., and Spagnolo, G. S. (1996). Generalized bessel-gauss beams. *Journal of Modern Optics*, **43**(6), 1155–1166.

Balkcum, A., Ellis, R., Boyd, D., and Guharay, S. (1992). Generation of millimeter wave gaussian beams and their propagation in a dielectric waveguide. *International journal of infrared and millimeter waves*, **13**(9), 1321–1340.

Belafhal, A. and Ibnchaikh, M. (2000). Propagation properties of hermite-cosh-gaussian laser beams. *Optics Communications*, **186**(4), 269–276.

Campbell, J. and DeShazer, L. (1969). Near fields of truncated-gaussian apertures. *JOSA*, **59**(11), 1427–1429.

Cazzoli, G., Cludi, L., Degli Esposti, C., and Dore, L. (1992). Lamb-dip absorption spectroscopy in the far infrared region using a laser sideband spectrometer. *Journal of Molecular Spectroscopy*, **151**(2), 378–383.

Chu, X., Ni, Y., and Zhou, G. (2007). Propagation of cosh-gaussian beams diffracted by a circular aperture in turbulent atmosphere. *Applied Physics B: Lasers and Optics*, **87**(3), 547–552.

Chu, X., Qiao, C., and Feng, X. (2010). The effect of non-kolmogorov turbulence on the propagation of cosh-gaussian beam. *Optics Communications*, **283**(18), 3398–3403.

Degnan, J. J. (1973). Waveguide laser mode patterns in the near and far field. *Applied optics*, **12**(5), 1026–1030.

DErrico, A., Maffei, M., Piccirillo, B., De Lisio, C., Cardano, F., and Marrucci, L. (2017). Topological features of vector vortex beams perturbed with uniformly polarized light. *Scientific reports*, **7**, 40195,

Franek, J. et al. (2017). Numerical treatment of the spatio-temporal electromagnetic beam-wave packet. *Journal of Electrical Engineering*, **68**(2), 109–116.

Gao, Z. and Lü, B. (2007). Phase-flipped hermite–gaussian beams and their propagation beyond the paraxial approximation. *Optics Communications*, **279**(1), 130–140.

Gutiérrez-Vega, J. C. and Bandres, M. A. (2005). Helmholtz–gauss waves. *JOSA A*, **22**(2), 289–298.

Harris, M. R. (1987). Large mode radius resonators. *Closed-Cycle, Frequency-Stable CO2 Laser Technology*, 23-31.

Hofstra, R. M., Goor, F., and Witteman, W. J. (1996, August)). Beam divergence studies on a long-pulse xecl excimer laser. *In High-Power Lasers: Gas and Solid State Lasers*, **2788**, 116-126.

Hussain, M. G. (2002). Principles of space-time array processing for ultrawide-band impulse radar and radio communications. *IEEE transactions on vehicular technology*, **51**(3), 393–403.

Kent, J. T., Mohammadzadeh, M., and Mosammam, A. M. (2011). The dimple in gneiting's spatial-temporal covariance model. *Biometrika*, **98**(2), 489–494.

Lorenser, D., Yang, X., and Sampson, D. D. (2013). Accurate modeling and design of graded-index fiber probes for optical coherence tomography using the beam propagation method. *IEEE Photonics Journal*, **5**(2), 3900015–3900015.

Matizen, Y. É. and Troitskiĭ, Y. V. (1987). Formation of non-gaussian light beams with the aid of a spatially inhomogeneous amplitude filter. *Soviet Journal of Quantum Electronics*, **17**(7), 886.

Mohammadzadeh, M., Omidi, M., and Mateu, J. (2015). A new family of spatio-temporal covariance functions with no dimple. In *Proceedings of the 17th Annual Conference of the International Association for Mathematical Geosciences*, 5–13. Freiberg, Germany.

Mosammam, A. (2015). The reverse dimple in potentially negative-value space–time covariance models. *Stochastic environmental research and risk assessment*, **29**(2), 599–607.

Ohtsuka, Y., Arima, Y., and Imai, Y. (1985). Acoustooptic 2-d profile shaping of a gaussian laser beam. *Applied optics*, **24**(17), 2813–2819.

Stuut, S. and Sargent, M. (1984). Effects of gaussian-beam averaging on phase conjugation and beat-frequency spectroscopy. *JOSA B*, **1**(1), 95–101.

Tao, R., Si, L., Ma, Y., Zhou, P., and Liu, Z. (2012). Relay propagation of partially coherent cosh-gaussian beams in non-kolmogorov turbulence. *Progress In Electromagnetics Research*, **131**, 495–515.

Walde, M., Jost, A., Wicker, K., and Heintzmann, R. (2017). Engineering an achromatic bessel beam using a phase-only spatial light modulator and an iterative fourier transformation algorithm. *Optics Communications*, **383**, 64–68.

Wang, Z., Zhang, Z., Xu, Z., and Lin, Q. (1997). Space-time profiles of an ultrashort pulsed gaussian beam. *IEEE journal of quantum electronics*, **33**(4), 566–573.

Yang, B., Trebbia, J., Baby, R., Tamarat, P., and Lounis, B. (2015). Optical nanoscopy with excited state saturation at liquid helium temperatures. *Nature Photonics*, **9**(10), 658–662.

Zeng-Hui, G. and Bai-Da, L. (2008). Nonparaxial propagation of phase-flipped gaussian beams. *Chinese Physics B*, **17**(3), 943–949.

Zhou, G. (2011). Propagation of a higher-order cosh-gaussian beam in turbulent atmosphere. *Optics express*, **19**(5), 3945–3951.

Ziolkowski, R. W. and Judkins, J. B. (1992). Propagation characteristics of ultrawide-bandwidth pulsed gaussian beams. *JOSA A*, **9**(11), 2021–2030.